

He³ Scattering from Nickel and Zirconium Isotopes*

D. E. RUNDQUIST,† M. K. BRUSSEL, AND A. I. YAVIN

Department of Physics, University of Illinois, Urbana, Illinois

(Received 19 June 1967; revised manuscript received 4 January 1968)

Angular distributions for elastic and inelastic He³ scattering from Ni⁵⁸, Ni⁶⁰, Ni⁶¹, Ni⁶⁴, Zr⁹⁰, Zr⁹¹, Zr⁹², and Zr⁹⁴ targets have been compiled at an incident beam energy of 25 MeV. Optical-model fits were obtained to the He³ elastic scattering angular distributions. Collective-model distorted-wave calculations were made for the inelastic scattering, utilizing the parameters obtained from the optical-model analysis of the elastic scattering, and deformation parameters were extracted. The inelastic transitions in Ni⁶¹ are interpreted by the core-excitation model.

I. INTRODUCTION

THE use of the He³ particle as a nuclear probe has become increasingly important in recent years. Reactions induced by He³ projectiles should in many ways be similar to those induced by α particles; for example, both are often characterized as surface reactions because of their complex compositions. However, the He³ nucleus has a spin of ½, an isospin of ½, and is more loosely bound than the α particle. Therefore, its detailed interaction with nuclei is expected to have its own unique identity—one which merits elucidation.

The simplest reaction to investigate with He³ particles is elastic scattering. From a study of elastic scattering one can begin to establish a phenomenological optical potential for its interaction with nuclei. Such a potential is necessary for the analyses of more complicated He³ interactions. Perhaps the most simple nonelastic interaction to investigate is inelastic scattering. From a study of this process, one can hopefully define more precisely the He³-nucleus optical potential and begin to better understand the nature of the He³ particle in inducing nuclear transformations. It is well known that α particles, for example, tend to preferentially excite low-lying 2⁺ and 3⁻ collective states of even-even nuclei.¹ It is of interest to verify the conjecture that He³ particles would behave similarly.

We present here an account of our experimental data for elastic and inelastic scattering of He³ nuclei from nickel and zirconium isotopes. These data are analyzed via the optical model and its collective model generalization in the distorted-wave Born approximation (DWBA).

II. THEORY

The exposition of the general distorted-wave theory as it applies to inelastic scattering has been given by several authors.² In this section we present a summary

* Supported in part by the U. S. Office of Naval Research under Contract No. 00014-67-A-0305-0005.

† Present address: Department of Physics, University of Michigan, Ann Arbor, Mich.

¹ R. H. Bassel, G. R. Satchler, R. M. Drisko, and E. Rost, Phys. Rev. 128, 2693 (1962); J. S. Blair, Argonne National Laboratory Report No. ANL-6878, p. 143 (unpublished).

² W. Tobocman, *Theory of Direct Nuclear Reactions* (Oxford University Press, London, 1961). R. H. Bassel, R. M. Drisko, and G. R. Satchler, Oak Ridge National Laboratory Report No. 3240, 1962 (unpublished); G. R. Satchler, Nucl. Phys. 55, 1 (1964).

of this theory that is specifically applicable to the present experiment.

The DWBA transition amplitude for the general reaction $A(ab)B$ has the form²

$$T_{\text{DW}} = \int d\mathbf{r}_{aA} \int d\mathbf{r}_{bB} \chi_{bB}^{(-)*}(\mathbf{k}_{bB}, \mathbf{r}_{bB}) \times \langle \psi_b \psi_B | V | \psi_a \psi_A \rangle \chi_{aA}^{(+)}(\mathbf{k}_{aA}, \mathbf{r}_{aA}), \quad (1)$$

where \mathbf{r}_{iI} symbolizes the displacement of particle i from nucleus I . The distorted waves $\chi^{(-)}$ and $\chi^{(+)}$ are solutions of the Schrödinger equation

$$[\nabla^2 + k^2 - (2\mu/\hbar^2)\bar{V}(r) - 2k\eta/r]\chi(\mathbf{k}, \mathbf{r}) = 0, \quad (2)$$

$\eta = Z_1 Z_2 e^2 / \hbar v$. The superscript on the wave function distinguishes the appropriate asymptotic boundary condition that defines the wave function. $\bar{V}(r)$ is the optical model potential, μ is the reduced mass, and k is the relative momentum for a given channel. The factor $\langle \psi_b \psi_B | V | \psi_a \psi_A \rangle$ is the matrix element of the interaction taken between the internal states of the nuclei. This factor contains all of the information on nuclear structure, angular-momentum selection rules, and the type of reaction considered.

The optical-model potential is taken to be local and to have the Woods-Saxon form

$$\bar{V}(r) = -V_r \{1 + \exp[(r - r_r A^{1/3})/a_r]\}^{-1} - iW_v \{1 + \exp[(r - r_i A^{1/3})/a_i]\}^{-1}, \quad (3)$$

where the six parameters V_r , r_r , a_r , W_v , r_i , and a_i are determined by analysis of the elastic scattering (see Sec. IV).

In this work, we characterize the low-lying excited states of the target as collective vibrations. The internal matrix element appropriate for exciting a one-phonon surface oscillation in the target nucleus is obtained¹ by deforming the spherical potential $\bar{V}(r)$. To first order in the multipole deformation parameter β_l , the nonspherical part of the potential has a matrix element of the form

$$\langle \psi_b \psi_B | V | \psi_a \psi_A \rangle \sim i^l \frac{(2s_a + 1)^{1/2}}{(2l + 1)^{1/2}} \beta_l \left\{ \frac{V_r R_r}{a_r} \times \frac{d}{dx_r} [1 + e^{x_r}]^{-1} + i \frac{W_v R_i}{a_i} \frac{d}{dx_i} [1 + e^{x_i}]^{-1} \right\} Y_l^m. \quad (4)$$

Here $x_j \equiv (r - r_j A^{1/3})/a_j$, where the subscript j may assume the role of r (real) or i (imaginary), and s_a is the spin of the scattered particle. The real and imaginary parts of the potential are assumed to be deformed equally. The angular-momentum transfer and parity change are determined by the multipole order l .

In this treatment, the optical-model analysis of the elastic scattering completely determines the inelastic scattering. We assume here that the distorted wave functions for the entrance and exit channels are determined by the optical-model parameters which fit the observed elastic scattering. Assuming vibrational collective oscillations, β_l represents the root-mean-square deformation in the ground state due to zero-point oscillations.¹ It is determined for a given transition by normalizing the theoretical angular distribution to the experimental angular distribution.

A strong coupling between the ground state and one or more excited states might seem to invalidate the treatment by the first-order Born approximation. For a deformation greater than $\beta_l = 0.2$, the DWBA treatment could seriously overestimate the cross section.³ However, the usual procedure of employing optical-model parameters in DWBA calculations for inelastic scattering makes this treatment valid for larger values of β_l than might be expected.⁴ The magnitudes of the deformations in Ni and Zr are within the accepted range for a distorted-wave treatment.

For simplicity, local potentials were used in the calculations despite expectations that the optical-model potential should be nonlocal.⁵ Nonlocality effects have been studied, and lead to small reductions in the predicted cross section.⁶ Hence the deformations reported here may be slightly overestimated.

The DWBA calculations were performed with the code JULIE,⁷ This code has an option for including Coulomb excitation of collective states.¹ This excitation mode was included, except where noted, in the present distorted-wave calculations.

III. EXPERIMENTAL APPARATUS AND PROCEDURE

We briefly describe the equipment used in these measurements. More details are to be found in Ref. 8.

A 25-MeV He³ beam was provided by the University of Illinois cyclotron.⁹ Beam currents of up to 2 μ A were used on target. These large currents were available partially because of the efficient beam extraction from the cyclotron, but more particularly because of the use of

a reclaiming system, which collected and purified the helium gas. Gas pumped unpurified from the cyclotron was initially stored in containers and later, at a convenient time, was circulated through a trap which had been cooled to liquid-He temperature. Non-He contaminants were thereby condensed out, and only pure He gas passed through the trap. Newly purchased He gas was also processed in this way, so that contaminants such as water vapor, which were found in this gas, were eliminated. Not only did use of this system render the cyclotron operation economical from the viewpoint of He³ consumption, but perhaps, more importantly, it allowed the cyclotron ion source to operate stably and efficiently.

The targets used in these measurements were self-supporting foils obtained from the Oak Ridge National Laboratory Isotopes Sales Division.

Particles scattered from the targets in our 28-in.-diam scattering chamber were detected with surface-barrier detectors. Angular-distribution measurements were made at 2 $\frac{1}{2}$ -deg intervals between 7 $\frac{1}{2}$ and 90 deg. The data reduction was done largely with use of digital-computer programs.¹⁰

IV. EXPERIMENTAL RESULTS AND ANALYSIS

A. Elastic Scattering

The ratio of the elastic scattering differential cross section to the Rutherford cross section (in the c.m. system) as a function of angle for the nine isotopes studied in this experiment are plotted in Figs. 1 and 2. These curves are mainly characterized by their average slopes. The solid curves in the figures are optical-model fits to the data.

The optical-model analysis was conducted under guidelines implied by previous analyses of He³ elastic scattering data.^{11,12} In these analyses a complex potential was used, having radius and diffuseness parameters for the imaginary potentials 10–20% larger than for the real potentials. The well depths for the real and imaginary potentials were approximately equal to the sum of the accepted well depths for the individual nucleons. Following a common procedure,¹³ an attempt was made to find a single set of geometrical parameters that would fit all of the Ni and Zr elastic scattering data. Only small differences in the real and imaginary well-depth parameters were permitted.

The automatic search routine of the code JTB3¹⁴ was

³ B. Buck, Phys. Rev. **130**, 712 (1963).

⁴ F. G. Perey and G. R. Satcher, Phys. Rev. Letters **5**, 212 (1963).

⁵ F. G. Perey and B. Buck, Nucl. Phys. **32**, 353 (1962).

⁶ F. G. Perey and A. M. Sarius, Nucl. Phys. **70**, 225 (1965).

⁷ Written by R. M. Drisko, Oak Ridge National Laboratory.

⁸ M. K. Brussel, D. E. Rundquist, and A. I. Yavin, Phys. Rev. **140**, 838 (1965).

⁹ J. S. Allen, S. Chatterjee, L. E. Ernest, and A. I. Yavin, Rev. Sci. Instr. **31**, 813 (1960).

¹⁰ Written by M. Kellogg and D. E. Rundquist.

¹¹ E. R. Flynn and R. H. Bassel, Phys. Rev. Letters **15**, 168 (1965); R. H. Siemssen, T. H. Braid, D. Dehnhard, and B. Zeidman, Phys. Letters **18**, 155 (1965).

¹² B. W. Ridley, E. F. Gibson, and J. J. Kraushaar, Bull. Am. Phys. Soc. **11**, HA2 (1966); and J. J. Kraushaar (private communication).

¹³ P. E. Hodgson, in *Comptes Rendus du Congrès International de Physique Nucléaire, II*, edited by P. Gungenberger (Centre National de Recherche Scientifique, Paris, 1964), Vol. I, p. 257.

¹⁴ Written by F. G. Perey, Oak Ridge National Laboratory.

used for the optical-model analysis. With this code, the elastic scattering is computed by solving the Schrödinger equation with the optical potential \bar{V} , and is compared with the experimental results. A best fit to the data is obtained by varying the optical parameters in such a manner as to minimize the quantity

$$\chi^2 = \sum_{i=1}^N \left[\frac{\sigma_{th}(\theta_i) - \sigma_{expt}(\theta_i)}{\Delta\sigma_{expt}(\theta_i)} \right]^2, \quad (5)$$

where σ is the theoretical (th) or experimental (expt) differential cross section at the scattering angle θ_i , and $\Delta\sigma_{expt}$ is the uncertainty associated with σ_{expt} .

Starting with parameters that were approximately those given by the University of Colorado group,¹² we found that reasonable fits to the data could be obtained. The final search procedure was to vary the real and imaginary central potential parameters (V_r and W_v , respectively), all other parameters being held fixed. Spin-orbit and surface-absorption potentials were set equal to zero after it was found that for nonzero values the cross sections at large scattering angles oscillated more than the experimental data indicated.

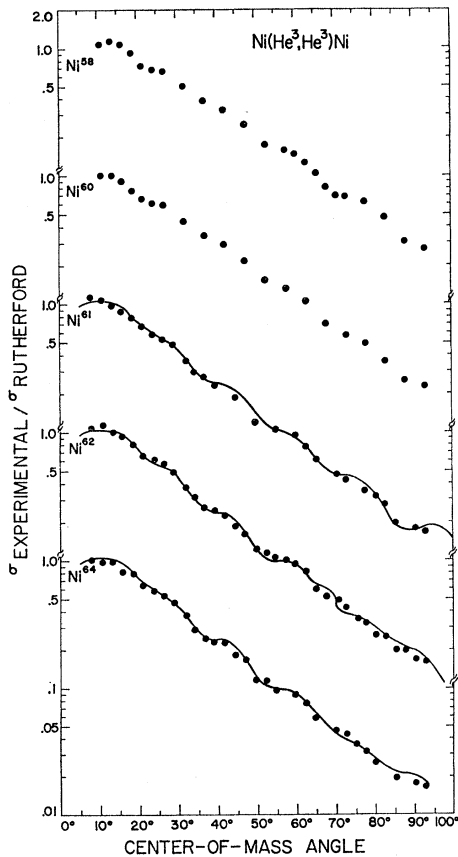


FIG. 1. The ratios of the Ni elastic scattering differential cross sections in the c.m. system to the Rutherford cross section plotted as a function of the c.m. angle. The solid curves represent optical-model fits to the experimental data.

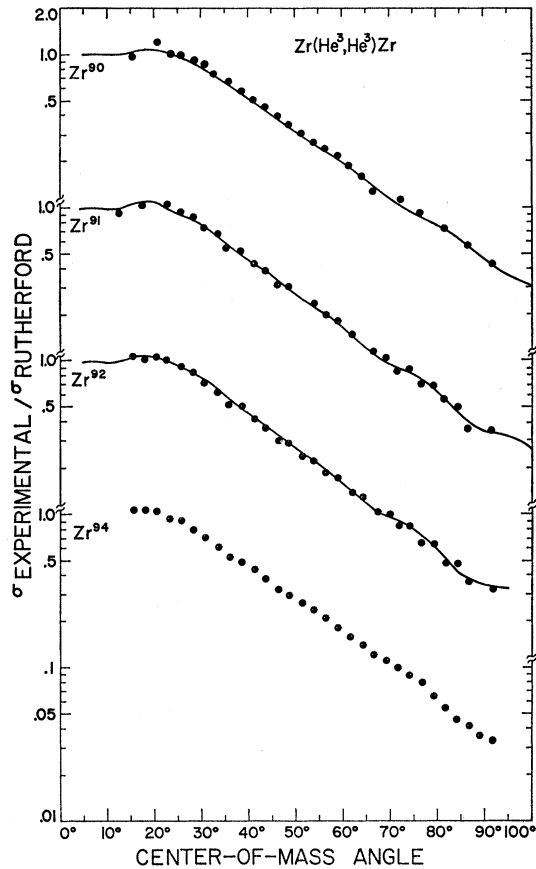


FIG. 2. The ratios of the Zr elastic scattering differential cross sections in the c.m. system to the Rutherford cross section plotted as a function of the c.m. angle. The solid curves represent optical-model fits to the experimental data.

The optical-model fits to the experimental elastic scattering data of Ni⁶¹, Ni⁶², and Ni⁶⁴ are shown in Fig. 1. Similar fits were obtained to the Ni⁵⁸ and Ni⁶⁰ data. However, for the latter cases, the real well-depth parameter V_r was approximately 90 MeV, whereas DWBA calculations for inelastic scattering preferred a deeper well depth. (See the discussion below.) χ^2/N for the fits shown in Fig. 1 are listed in Table I. These χ^2/N values were not the minimum values obtained for the individual isotopes. The minimum χ^2/N values were obtained by searching for a best fit with all parameters simultaneously. However, because the individual parameters pertaining to the best values for χ^2/N varied widely among the isotopes, and because the minimum χ^2/N differed only by a factor of about 3 from the values obtained using fixed geometrical parameters, the latter parameters were used in the distorted-wave calculations.

Optical-model fits to Zr⁹⁰, Zr⁹¹, and Zr⁹² elastic scattering data are shown in Fig. 2. No satisfactory set of optical-model parameters was found from searches on the Zr⁹⁴ data. In particular, the value for W_v was found to be in large disagreement with values obtained for Zr⁹⁰, Zr⁹¹, and Zr⁹². Therefore, the value for W_v that is

TABLE I. He³ optical-model parameters used in the DWBA calculations. The parameter sets that have a value listed for χ^2/N were obtained from the optical-model analysis of the observed He³ elastic scattering data.

Isotope	V_r (MeV)	r_r (F)	a_r (F)	W_o (MeV)	r_i (F)	a_i (F)	r_e (F)	χ^2/N
Ni ⁵⁸	180	1.14	0.71	19.0	1.54	0.78	1.4	...
Ni ⁶⁰	180	1.14	0.71	19.0	1.54	0.78	1.4	...
Ni ⁶¹	178.47	1.14	0.71	19.52	1.54	0.78	1.4	1.344
Ni ⁶²	192.53	1.14	0.71	19.42	1.54	0.78	1.4	0.756
Ni ⁶⁴	187.44	1.14	0.71	18.60	1.54	0.78	1.4	1.245
Zr ⁹⁰	168.36	1.14	0.71	16.88	1.54	0.78	1.4	5.0
Zr ⁹¹	177.33	1.14	0.71	15.50	1.54	0.78	1.4	3.576
Zr ⁹²	179.45	1.14	0.71	14.95	1.54	0.78	1.4	4.392
Zr ⁹⁴	176.4	1.14	0.71	14.5	1.54	0.78	1.4	...

listed in Table I and used in the Zr⁹⁴ DWBA calculations was extrapolated from the W_o 's that were determined from the optical-model analysis of the Zr⁹⁰, Zr⁹¹, and Zr⁹² elastic scattering data. The χ^2/N values listed for Zr are somewhat larger than those listed for Ni. This is mainly due to the smaller uncertainty $\Delta\sigma_{\text{expt}}$ that was used.

B. Inelastic Scattering

We find that He³ inelastic scattering strongly excites collective states. Indeed, we found that in most cases the only distinguishable peaks in our spectra for reactions with negative Q values corresponded to the inelastic scattering transitions to 2⁺ and 3⁻ collective states.

We present the experimental angular distributions for inelastic scattering in Figs. 3–11. Excitation energies of the observed states are in good agreement with previous results.^{15,16}

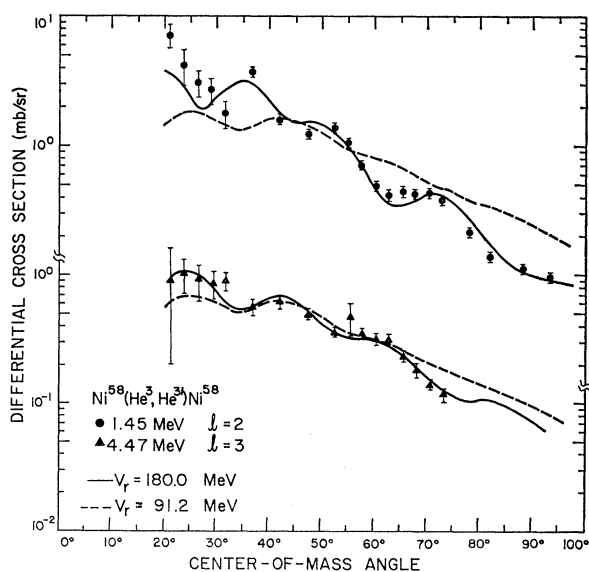


FIG. 3. Inelastic He³ differential cross sections for Ni⁵⁸. The smooth curves are DWBA predictions. The solid curve is for the optical-model parameters listed in Table II.

¹⁵ Nuclear Data Sheets, compiled by K. Way *et al.* (Printing and

In general, the angular distributions obtained from the Ni targets exhibit more structure than those from the Zr targets. This structure in the Ni inelastic scattering angular distributions is sufficient, for example, to demonstrate that Blair's phase rule,¹⁷ i.e., that angular distributions for transitions involving an orbital angular-momentum transfer of an even (odd) number of units will be out of (in) phase with the elastic scattering, is valid for these states. Figures 3, 6, and 7 illustrate the regular phase differences that exist between the 2⁺ and 3⁻ angular distributions; the elastic scattering data do not show sufficient angular structure for comparison purposes.

As mentioned previously, the optical-model fits to the elastic scattering data of Ni⁵⁸ and Ni⁶⁰ persistently converged to a real well depth V_r of approximately 90 MeV. This result was inconsistent with the results obtained for the other isotopes, where the real well depth was approximately 180 MeV. DWBA calculations were performed for both the 90-MeV set of optical-model parameters and a "consistent" set of parameters with

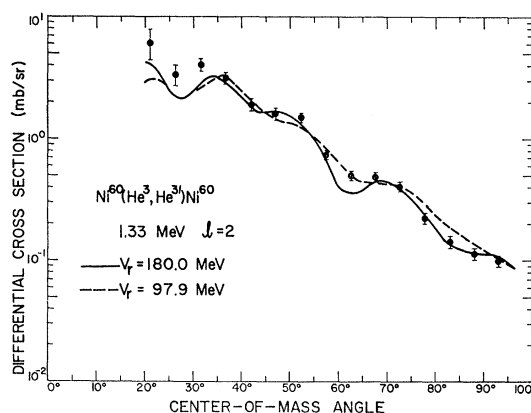


FIG. 4. Inelastic He³ differential cross sections for Ni⁶⁰. The solid DWBA curve was determined from the optical parameters listed in Table I.

Publishing Office, National Academy of Sciences–National Research Council, Washington, 25, D. C., 1962).

¹⁶ H. W. Broek, Phys. Rev. **130**, 1914 (1963); H. W. Broek and J. L. Yntema, *ibid.* **138**, B334 (1965).

¹⁷ J. S. Blair, Phys. Rev. **115**, 928 (1959).

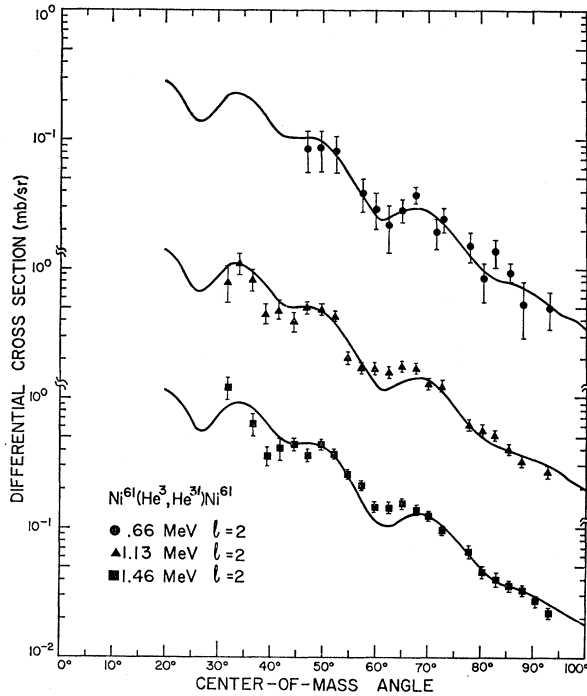


FIG. 5. Inelastic He³ differential cross sections for Ni⁶¹. The solid curves are $l=2$, DWBA predictions.

$V_r=180$ MeV and $W_0=19.0$ MeV. In Fig. 3 it is apparent that the consistent set of parameters predicts a better fit to the Ni⁵⁸ 2⁺ and 3⁻ angular distributions than do the shallower well parameters. Specifically, the relatively deep oscillations of the 2⁺ curve are not predicted by calculations using the shallow well. The sensi-

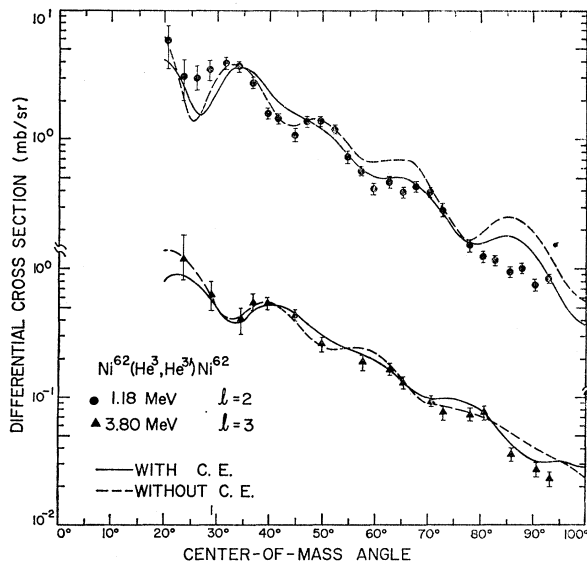


FIG. 6. Inelastic He³ differential cross sections for Ni⁶². The dashed curves are DWBA predictions without the inclusion of Coulomb excitation.

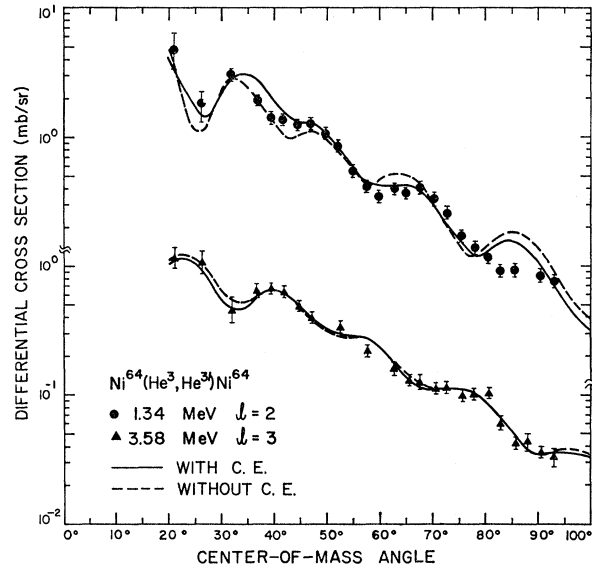


FIG. 7. Inelastic He³ differential cross sections for Ni⁶⁴. The dashed curves are DWBA predictions without the inclusion of Coulomb excitation.

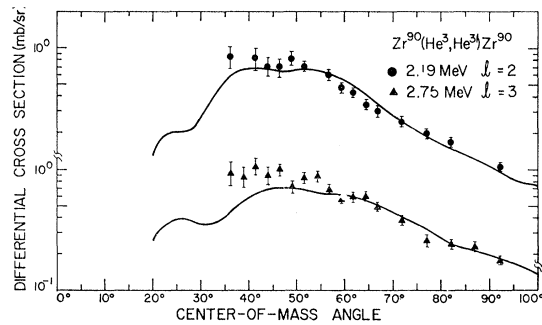


FIG. 8. Inelastic He³ differential cross sections for Zr⁹⁰. The smooth curves are DWBA predictions.

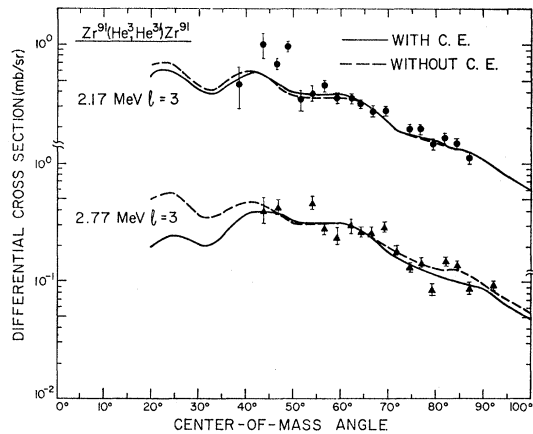


FIG. 9. Inelastic He³ differential cross sections for Zr⁹¹. These probably include unresolved states. The dashed curves are DWBA predictions without the inclusion of Coulomb excitation.

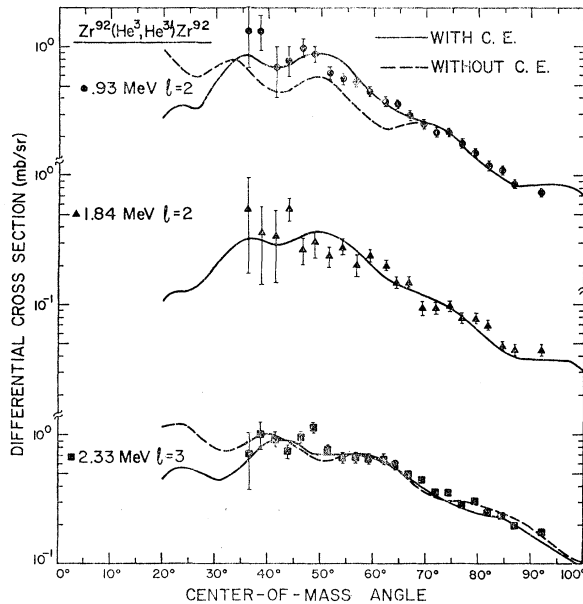


FIG. 10. Inelastic He^3 differential cross sections for Zr^{92} . The dashed curves are DWBA predictions without Coulomb excitation.

tivity to the well depth is not so pronounced for the Ni^{60} 2^+ angular distribution in Fig. 4, but the deep well curve does match the data better for angles greater than 65 deg. The 3^- state in Ni^{60} was also observed, but the data were insufficient for analysis. The results suggest that the simplistic picture where the He^3 optical-model potential is the sum of free nucleon potentials has some validity. Optical-model fits to proton data typically use

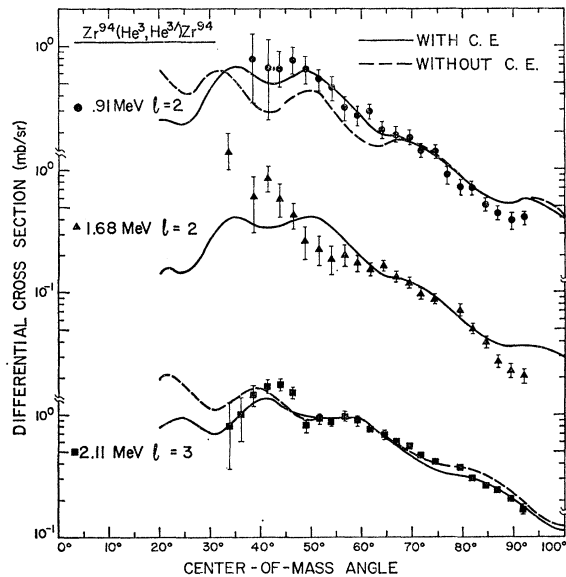


FIG. 11. Inelastic He^3 differential cross sections for Zr^{94} . The dashed curves are DWBA predictions without Coulomb excitation. The level at 1.68 MeV is probably not a single-phonon 2^+ state.

well depths of about 50 MeV. It is perhaps noteworthy that optical-model fits to the Ni^{58} and Ni^{60} elastic-scattering data were found with $V_r \approx 180$ MeV for a smaller real potential radius r_r of 1.05 F.

The distorted-wave predictions with and without the inclusion of Coulomb excitation are plotted for the reactions $\text{Ni}^{62}(\text{He}^3, \text{He}^3)\text{Ni}^{62}$ and $\text{Ni}^{64}(\text{He}^3, \text{He}^3)\text{Ni}^{64}$ in Figs. 6 and 7, respectively. It is apparent from the plots that Coulomb excitation plays a minor role in He^3 inelastic scattering on Ni at an incident beam energy of 25 MeV. The inclusion of Coulomb excitation seems to smooth out the predicted angular distribution, but the fit to the experimental results is not noticeably im-

TABLE II. Nickel deformation parameters extracted from fitting the DWBA curves to the measured angular distributions. (A) and (B) represent the two optical parameter sets used in the DWBA calculations for Ni^{58} and Ni^{60} . For (A), $V=180$ MeV, for (B) $V \approx 90$ MeV. The DWBA calculations from which β_1 was extracted included Coulomb excitation.

Isotope	E	J^π	β_1	β_1	$\beta_1 R_1$
Ni^{58}	1.45	2^+	0.22 (A)	0.187 ^a	1.33 (A)
			0.26 (B)	0.17 ^b	1.57 (B)
	4.5	3^-		0.24 ^c	
				0.19 ^d	
				0.15 ^e	
				0.10 ^f	
Ni^{60}	1.33	2^+	0.22 (A)	0.211 ^a	1.33 (A)
			0.21	0.21 ^b	1.27 (B)
	3.8	3^-		0.28 ^c	
				0.22 ^d	
				0.18 ^b	
				0.30 ^f	
Ni^{61}	0.66	$\frac{1}{2}$	0.184		1.12
	1.13	$\frac{3}{2}, \frac{5}{2}^-$	0.177		1.07
	1.46	$\frac{1}{2}$	0.183		1.11
Ni^{62}	1.18	2^+	0.22	0.193 ^a	1.31
				0.30 ^c	
Ni^{64}	3.8	3^-	0.14	0.24 ^c	0.865
	1.34	2^+	0.20	0.192 ^a	1.23
	3.58	3^-	0.15		0.92

^a Coulomb excitation [P. Stelson and L. Grodzins, Nucl. Data 1, 21 (1965), Sec. A, and references therein].

^b (α, α') [G. R. Satchler, Nucl. Phys. 70, 177 (1965)].

^c (p, p') [Ref. 20].

^d (p, p') [M. P. Fricks and G. R. Satchler, Phys. Rev. 139, B567 (1965)].

^e (He^3, He^3) [Ref. 11].

^f (d, d') [Ref. 30].

proved. However, the deformation parameter β_1 did agree better with other results if Coulomb-excitation effects were incorporated in the calculation.

Table II lists the values of the extracted deformation parameters for Ni. A few values of β_1 reported in the literature are also included. The nuclear spins listed for the excited 2^+ and 3^- states have all been previously established.^{15,16} The last column of Table II shows the deformation distances $\beta_1 R_1$. Blair¹⁸ has emphasized the importance of this quantity in comparing results ob-

¹⁸ J. S. Blair, in *Proceedings of the Conference on Direct Interactions and Nuclear Reaction Mechanisms, Padua, 1962*, edited by E. Clementel and C. Villi (Gordon and Breach Science Publishers, Inc., New York, 1963).

tained by different methods. Our results for β_l are in good agreement with previously published results obtained from other reactions. Differences do exist, but, as Dickens *et al.*¹⁹ have pointed out, insofar as the optical potential is a property of both projectile and target nuclei, there seems no *a priori* reason to believe that β_l should be identical for different inelastic scattering reactions.

An interesting aspect of our results is that β_2 and β_3 have a narrow range of values for the even-even nuclei. For the 2^+ states the values of β_2 lie between 0.20 and 0.22. A similar result has been found for the β_2 's determined by other methods such as Coulomb excitation.²⁰ The β_3 lie between 0.14 and 0.18.

The values of β_l listed for Ni⁶¹ stem from an application of the excited-core model for inelastic reactions.²¹⁻²³ The excited-core model assumes that some of the energy levels for odd-*A* nuclei can be interpreted as resulting from the coupling of the odd nucleon to an excited state of the even-even core. The spin of the ground state (J_0) of the odd nucleus is assumed to be due to the angular momentum of the odd nucleon. There should also be a low-lying multiplet of excited states in the odd nucleus due to the coupling of this spin with the spin of the first (collective) excited state of the core (J_c). The spin and parity of the ground state of Ni⁶¹ is $J^\pi = \frac{3}{2}^-$; the first excited state of the Ni⁶⁰ core has $J^\pi = 2^+$. Therefore, the low-lying multiplet should contain states with J^π of $\frac{1}{2}^-$, $\frac{3}{2}^-$, $\frac{5}{2}^-$, and $\frac{7}{2}^-$.

We observe inelastic scattering to levels at 0.66, 1.13, and 1.46 MeV, which we assume to be the core-excitation model quartet, the 1.13-MeV level being an unresolved doublet. These levels should, therefore, have spins of $\frac{1}{2}^-$, $\frac{3}{2}^-$, $\frac{5}{2}^-$, and $\frac{7}{2}^-$. Evidence for spins of levels in these regions of excitation are not conclusive. However, in the Ni⁶⁰(*d,p*)Ni⁶¹ reaction, Fulmer *et al.*²⁴ have seen weak, equivalently excited, levels at energies of 0.654, 1.139, and 1.454 MeV, and they assign *l* values of 1, 3, and 3 to these levels, respectively. Moreover, the level at 1.139 MeV is indicated as being not clearly resolved from an *l*=1 level. Fulmer and Daehnick,²⁵ in the Ni⁶²(*d,t*)Ni⁶¹ reaction, have reported levels at 0.65, 1.11, 1.17, and 1.45 MeV with spins of $\frac{1}{2}^-$, ($\frac{3}{2}^-$), $\frac{5}{2}^-$, and ($\frac{7}{2}^-$), respectively. Sherr *et al.*²⁶ in the Ni⁶²(*p,d*)Ni⁶¹ reaction have reported an unresolved doublet at 1.17 MeV with *l*=1 and possibly *l*=3 components. In the

following paper²⁷ we also present some evidence to indicate the existence of an *l*=3 level near this excitation energy. It should be noted that the $\frac{3}{2}^-$ level of the quartet should have its strength diminished by virtue of admixture of this state with the Ni⁶¹ ground state, which possesses the same spin and parity.

Assuming the validity of the core-excitation model, the center of gravity of the multiplet should be at the same excitation energy as the core-excited state (the 2^+ at the 1.33 MeV in Ni⁶⁰). Specifically,

$$E_c = \sum_i \frac{E_i(2J_i+1)}{(2J_0+1)(2J_c+1)}, \quad (6)$$

where J_i is the spin of the *i*th excited state of the multiplet in Ni⁶¹. If we use the excitation energies shown in Fig. 5, Eq. (6) yields $E_c = 1.22$ MeV, a not unreasonable result. Similarly, assuming that the extra nucleon contributes negligibly to the scattering, the excitation cross section summed over each member of the multiplet should equal the cross section for the excitation of the core state. For example, at a scattering angle of 65 deg, the cross section for the 2^+ state in Ni⁶⁰ is 0.48 mb/sr. The sum of the multiplet cross sections at the same scattering angle is 0.35 mb/sr, again a not unreasonable result.

Because we are assuming here that the excitation mechanism is due to the core alone, we expect to see similar angular distributions for the 2^+ state in Ni⁶⁰ and the corresponding states in Ni⁶¹. Moreover, the angular-momentum transfer in the inelastic transition to each member of the multiplet should be two units. In Fig. 5 we see that the angular distributions are indeed similar, and that all of the three angular distributions are well fitted by DWBA predictions for *l*=2. These fits certainly imply that the angular-momentum transfer cannot be 3, for if that were the case the theoretical and experimental curves would be out of phase. The only strong states observed in these inelastic studies corresponded to collective quadrupole or octupole excitations. Therefore, to the extent that these are collective states, they most likely correspond to quadrupole oscillations.

Deformation parameters were also extracted from our data using the DWBA formalism. The excited-core model predicts that the differential cross section for a member of the multiplet with spin *J* is given by¹⁸

$$\left. \frac{d\sigma}{d\Omega} \right|_{\text{odd nucl}} = \frac{2J+1}{(2J_0+1)(2J_c+1)} \left. \frac{d\sigma}{d\Omega} \right|_{\text{core}}. \quad (7)$$

The extraction of β_l immediately follows upon substituting $\beta_l^2 \sigma_{\text{DWBA}}$ for $(d\sigma/d\Omega)_{\text{core}}$. The consistency of the β_2 's extracted in this manner is evident from Table II.

All of this evidence indicates that the excited-core

¹⁹ J. K. Dickens, F. G. Perey, and G. R. Satchler, Nucl. Phys. **73**, 529 (1965).

²⁰ S. F. Eccles, H. T. Lutz, and V. A. Madsen, Phys. Rev. **141**, 1067 (1966).

²¹ R. D. Lawson and J. L. Uretsky, Phys. Rev. **108**, 1300 (1957).

²² A. De Shalit, Phys. Rev. **122**, 1530 (1961).

²³ F. G. Perey, R. J. Silva, and G. R. Satchler, Phys. Rev. Letters **4**, 25 (1963).

²⁴ R. H. Fulmer, A. L. McCarthy, B. L. Cohen, and R. Middleton, Phys. Rev. **133**, B955 (1964).

²⁵ R. H. Fulmer and W. W. Daehnick, Phys. Rev. **139**, B579 (1965).

²⁶ R. Sherr, E. Rost, and M. E. Rickey, Phys. Rev. Letters **12**, 420 (1964).

²⁷ D. E. Rundquist, M. K. Brussel, and A. I. Yavin, following paper, Phys. Rev. **168**, 1296 (1968).

model provides a possible interpretation of these inelastic states in Ni^{61} . However, it is interesting to note that a possible configuration in the 2^+ core wave function $(p_{3/2})_{J=2}^2$ cannot be coupled with a $p_{3/2}$ neutron to form these excited states.

The distorted-wave predictions for the inelastic 2^+ and 3^- angular distributions of Zr^{90} are presented in Fig. 8. Although the fits to the experimental data must be regarded as adequate, there does appear to be some discrepancy. A possible reason for this is that an improper choice of optical-model parameters has been made. The DWBA calculations shown in Fig. 8 employed the consistent set of parameters tabulated in Table I. Other calculations were performed with the set of optical-model parameters that corresponded to the best value of χ^2 , but agreement with the data was not noticeably improved.

Another more fundamental explanation for any disagreement between the theoretical predictions of the distorted-wave calculations and the experimental data for Zr lies in the possible inapplicability of the collective model. This is particularly relevant to the 2^+ state at 2.19 MeV in Zr^{90} . Many authors have discussed the low-lying levels of Zr^{90} in terms of a shell-model description.²⁸ In particular, the 2^+ state at 2.19 MeV is thought to be well described by two protons in the $g_{9/2}$ orbit. Presumably, the collective model is not appropriate for this state, and the fact that the fit to the data is not better is not surprising. The low value of the normalization constant (Table III) may lend support to this contention.

TABLE III. Zirconium deformation parameters extracted from fitting the DWBA curves to the measured angular distributions. All deformation parameters shown here were extracted from DWBA calculations that included Coulomb excitation.

Isotope	E	J^π	β_l	β_l	$\beta_l R_i$
Zr^{90}	2.19	2^+	0.10	0.066 ^a	0.69
				0.07 ^b	
	2.75	3^-	0.16	0.073 ^c	1.09
				0.074 ^d	
Zr^{91}	2.17	3			
	2.77	3			
Zr^{92}	0.93	2^+	0.10	0.106 ^a	0.70
				0.11 ^d	
	1.84	2^+	0.07	0.10 ^e	0.49
				0.048 ^a	
2.33	3^-	0.16	0.151 ^a	1.12	
			0.14 ^e		
Zr^{94}	0.91	2^+	0.086	0.11	0.60
	1.68	$+$			
	2.11	3^-	0.18		1.26

^a α, α' [H. Ogata, S. Tometa, M. Inone, Y. Okuma, and J. Kumabe, Phys. Letters 17, 280 (1965).]

^b p, p' [Ref. 28].

^c α, α' [Ref. 32].

^d Coulomb excitation [P. Stelson and L. Grodzins, Nucl. Data 1, 21 (1965), Sec. A, and references therein].

^e d, d' [Ref. 30].

²⁸ See, e.g., W. S. Gray, R. A. Kenefick, J. J. Kraushaar, and G. R. Satchler, Phys. Rev. 142, 735 (1966), and references therein.

Distorted-wave calculations for the Zr^{91} inelastic angular distributions are compared with the experimental data in Fig. 9. The inconsistency of the experimental points near 50 deg is believed to be due to carbon and oxygen contaminants in the target. Our experimental data and previously published results²⁹ imply that each of the curves is for a group of unresolved states. This is particularly true for the group at 2.77 MeV. The distorted-wave calculations were performed with the assumption that the excited-core model is applicable. For Zr^{91} we have assumed that the extra neutron is coupled to the excited 3^- core state of Zr^{90} . (This octupole transition was the strongest transition seen in Zr^{90} .) The dashed curves shown in the figure represent calculations without Coulomb excitation. The differences in the shapes of the theoretical angular distributions are small.

Distorted-wave angular distributions calculated for Zr^{92} employing the collective model are shown in Fig. 10. These predictions seem to be in better agreement with the experimental results than those for Zr^{91} and Zr^{90} . The experimental structure in the angular distribution is reproduced, and the general slope is predicted in all three cases. The discrepancy for points between 45 and 50 deg for the 3^- state at 2.33 MeV may be spurious, due to contaminants in the target.

It is somewhat surprising that the predicted distorted-wave angular distribution compares so well with the experimental results for the state at 1.84 MeV. $\text{Zr}^{92}(d, d')$ data³⁰ indicated that this state was a 2^+ member of a two-phonon triplet. One might then expect a different shape for the angular distribution than for that of the single-phonon state. On the other hand, Bingham *et al.*³¹ obtained a fit to (α, α') data, assuming a single-phonon excitation, while Broek *et al.*¹⁶ found a state at 1.9 ± 0.1 MeV that had an angular distribution which was definitely out of phase with the elastic angular distribution, and therefore implied a one-phonon excitation.

The β_l 's extracted by the normalization of the theoretical predictions to the experimental results of Zr^{92} are listed in Table III. It is noteworthy that the β_2 's for the first two excited states are small, especially for the state at 1.84 MeV.

The dashed curves in Fig. 10 represent distorted-wave calculations without the inclusion of Coulomb excitation. Coulomb effects are seen to be significant for the 2^+ state at 0.93 MeV. Without Coulomb excitation, the predicted angular distribution is in serious disagreement with the experimental angular distribution. As expected,³² this effect is more prominent for the 2^+ state than for the 3^- state.

²⁹ B. L. Cohen and O. V. Chubinsky, Phys. Rev. 131, 2184 (1963).

³⁰ R. K. Jolly, Phys. Rev. 139, B318 (1965).

³¹ C. R. Bingham, M. L. Halbert, and R. H. Bassel, Phys. Rev. 148, 1174 (1966).

³² R. H. Bassel, R. M. Drisko, G. R. Satchler, Oak Ridge National Laboratory Report No. 3240, 1962 (unpublished).

Distorted-wave predictions for inelastic scattering from Zr⁹⁴ are compared with experimental angular distributions in Fig. 11. The fits to the data are in reasonable agreement for the 2⁺ state at 0.91 MeV and the 3⁻ state at 2.11 MeV. The theoretical angular distribution for the positive-parity state at 1.68 MeV³³ is not reproduced by a $l=2$ angular distribution. A serious divergence exists for scattering angles less than 60 deg when the normalization is done as shown. This state, therefore, does not appear to be a one-phonon 2⁺ state, but is most likely a member of a two-phonon triplet. Further support for this assumption is based on the facts that its excitation energy is approximately twice that found for the first 2⁺ state and that its angular distribution is not only in significant disagreement with the theoretical prediction, but is also somewhat different from the experimental angular distribution for the first 2⁺ state.

Predicted angular distributions without the inclusion of Coulomb excitation are the same as in Zr⁹² and display similar discrepancies with the experimental data.

Comparison of the extracted deformation parameters for the Zr isotopes, Table III, reveal that all of the β_2 's are near 0.1. Moreover, they are all smaller than those extracted from the Ni data. The β_3 's for Zr⁹⁰, Zr⁹², and Zr⁹⁴ are approximately equal. The magnitudes of β_3 for Zr lie near the range of β_3 that was observed for Ni.

V. SUMMARY AND CONCLUSIONS

The (He³,He^{3'}) reaction has been found to be effective in exciting collective states in the Ni and Zr isotopes, similar to what has been found previously for (α,α') reactions.¹⁶ The single-phonon collective states are strongly excited, the quadrupole transitions being more

strongly excited in Ni, whereas the octupole transitions are more strongly excited in Zr.

The core-excitation model appears to explain, within the theoretical and experimental uncertainties, the observed states that were excited by the Ni⁶¹(He³,He^{3'}) reactions. The experimental uncertainties involved in the Zr⁹¹(He³,He^{3'}) transitions preclude any interpretation of these data by this model.

The optical-model analysis of the elastic scattering employed parameters which varied smoothly from isotope to isotope, and which, when employed in the DWBA calculations, provided reasonable fits to the data.

The collective-model DWBA analysis was straightforward and quite successful in fitting the observed angular distributions. The deformation parameters that were extracted from these fits are in general agreement with the deformation parameters that were obtained from other work. The magnitudes of the β_3 values are similar for the Ni and Zr isotopes. However, the values of β_2 were significantly smaller for the Zr isotopes than for the Ni isotopes.

ACKNOWLEDGMENTS

We would like to thank the Oak Ridge National Laboratory for the use of its computer facilities. We would particularly like to thank C. R. Bingham for his hospitality, and his invaluable assistance and guidance with the DWBA analysis. We wish also to thank R. M. Drisko for his help with the DWBA analysis and for several informative discussions. One of us (D.E.R.) would like to acknowledge the financial support of an Atomic Energy Commission Fellowship from the Oak Ridge Associated Universities during the initial period of this experiment. We also thank L. E. Ernest and the cyclotron staff for their cooperation in this experiment.

³³ R. K. Jolly, E. K. Lin, and B. L. Cohen, Phys. Rev. **128**, 2292 (1962).